Periodic structures generated in a cloud of cold atoms

D. V. Strekalov,* Andrey Turlapov, A. Kumarakrishnan,† and Tycho Sleator‡
Department of Physics, New York University, 4 Washington Place, New York, New York 10003
(Received 23 October 2001; revised manuscript received 10 May 2002; published 5 August 2002)

We have demonstrated a method of generation and real-time detection of nanostructures in a cold Rb cloud. These structures, which are periodic gratings of atomic density, appear as a result of interference of atoms diffracted by pulses of an optical standing wave of wavelength λ. We have detected structures of period $\lambda/2$ and $\lambda/4$. Calculations indicate that these density gratings have period $\lambda/2N$ for integer N. While the structures with the period $\lambda/2$ are easily detected by Bragg scattering of an optical probe beam, the shorter-period structures are not. For their detection we have developed a three-pulse echo method, in which the shorter-period gratings get converted into the structures with period $\lambda/2$, readily detected in real time. Applications related to lithography are discussed.

DOI: 10.1103/PhysRevA.66.023601 PACS number(s): 03.75.Be, 42.50.Md, 42.82.Cr

I. INTRODUCTION

Atom interferometry [1,2] is a new and rapidly developing area of physics. Over the last several years, interferometric techniques have been used for new and precise measurements of the earth's gravitational acceleration g [3–5], the gradient of g [6], $\hbar/m_{Cs}$ (where m_{Cs} is the mass of the cesium atom) [7,8], refractive index for matter waves in a gas [9], and frequencies of slow rotations [10,11]. In this work, we utilize techniques of atom interferometry and atom optics for creating small-scale periodic structures in a cloud of laser-cooled atoms. Our technique is readily applicable to atom beam lithography.

So far, several groups have demonstrated atom lithography using a single optical standing wave for manipulations on an atomic beam. Atomic structures of period $\lambda/2$ [12–15] and $\lambda/4$ [16] have been deposited onto a substrate, where λ is the optical wavelength. To form these sub-λ structures, atoms were focused into the minima of the potential created by the optical standing wave, which is set up perpendicular to the atomic beam. Earlier, Mossberg *et al.* [17] suggested that a grating of atomic *inversion*, having period $\lambda/2N$ for integer N, can be created using the effect of the grating echo they discovered. Mossberg *et al.* observed a $\lambda/2$ *inversion* grating in sodium vapor.

We report a method for creating modulation of the total atomic *density* with period $\lambda/2N$. In our experiments, which were performed in the time domain, a cloud of cold Rubidium atoms was irradiated by a sequence of optical standing-wave pulses. These standing-wave pulses diffract the atoms into a superposition of momentum states differing by $2\hbar k$ (twice the photon momentum). At certain times, atomic states with momenta that differ by $2N\hbar k$ coherently interfere, resulting in a density modulation (interference fringes) with period $\lambda/2N$. This resulting density modulation can be considered a type of *photon echo* [18,19]. Conceptually, our time-domain experiment is close to the space-domain experiment suggested by Dubetsky *et al.* [20], in which an atomic beam passes through several zones of atom-light interaction and each zone is analogous to a light pulse in our experiment.

Unlike the work of Mossberg *et al.*, we only manipulate atoms in the ground state and thus, the duration of our experiment is not limited by the lifetime of the atomic excited states. This allows us to explore the fundamental issues of matter-wave interference by carrying out the experiment over the times longer than the Talbot time [21], during which the phase associated with the energy transfer between the atom and the field becomes important.

The techniques discussed here may have direct application towards lithography. Periodic structures with periods a small fraction of an optical wavelength deposited on a substrate may serve as reflective diffraction gratings for ultraviolet and soft x-ray radiation. Our method will be good for this application because the density modulations we create are almost purely sinusoidal resulting in more efficient diffraction into fewer orders. In addition, because our technique is based on coherent light fields, the coherence length of any deposited structures would be very large. Another feature of this technique applied to atom lithography is that no subrecoil collimation of the atoms being deposited is needed (i.e., the atomic momentum distribution does not have to be narrower than $2\hbar k$). Using an uncollimated beam allows a larger flux of atoms and a correspondingly shorter deposition time.

As a first step, we formed and detected in real-time gratings of periods $\lambda/2$ and $\lambda/4$. We plan to employ our technique for the formation of gratings with periods $\lambda/6$, $\lambda/8$, etc., and to apply it to lithography with an atomic beam.

This paper is organized as follows: Section II gives a qualitative description of the experiment and explains the underlying physics; in Sec. III, the experimental apparatus is described; in Sec. IV, we discuss our experimental results; and Sec. IV presents a detailed theory of atomic density gratings generated by standing-wave pulses in a cold atomic cloud.

*Present address: JPL, M. S. 300-123, 4800 Oak Grove Drive, Pasadena, CA 91109.
†Present address: Department of Physics and Astronomy, York University, 4700 Keele Street, Toronto, Ontario, Canada M3J1P3.
‡Electronic address: tycho.sleator@nyu.edu

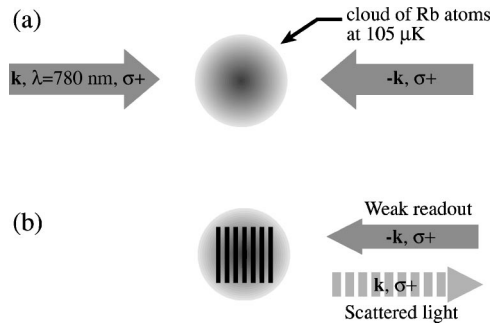

FIG. 1. Sketch of experiment: (a) A cloud of cold Rb atoms is illuminated by short pulses of a standing wave made of two counterpropagating waves of the same polarization; (b) to detect $\lambda/2$ grating in the cloud, we switch on a weak field in the mode $\mathbf{k}_2$, which is coherently scattered into the mode $\mathbf{k}_1$ by the density grating.

II. QUALITATIVE DESCRIPTION OF EXPERIMENT

A sketch of the experiment is shown in Fig. 1. A cloud of $\sim$100-μK ^{85}Rb atoms, prepared by laser-cooling techniques, is illuminated by three short pulses [Fig. 1(a)] of an off-resonant optical standing wave (SW) composed of two plane waves with identical polarizations traveling in opposite directions, $\mathbf{k}_1$ and $\mathbf{k}_2$ $(\mathbf{k}_1=-\mathbf{k}_2\equiv\mathbf{k})$.

For short times after a pulse (much less than the Talbot time), the effect of the standing wave is to focus the atoms towards the nodes (or antinodes) by the optical dipole force. For longer times after the pulse, the atomic motion must be treated quantum mechanically, and it is convenient to think of the standing-wave pulses as diffraction gratings for atomic de Broglie waves. We can describe the initial state of the atomic cloud as an incoherent mixture of atomic momentum states. To understand the effect of the pulse sequence on the atomic cloud, we may first compute the effect on an initial momentum state $|\mathbf{p}_0\rangle$ and then sum the result over the momentum distribution of the atomic cloud. The effect of a standing-wave pulse on the initial state $|\mathbf{p}_0\rangle$ is to create a superposition of momentum states that differ from $\mathbf{p}_0$ by multiples of the photon momentum difference $\hbar(\mathbf{k}_2-\mathbf{k}_1)=2\hbar\mathbf{k}\equiv\hbar\mathbf{q}$. This momentum exchange is a result of two-photon processes that bring the atomic internal ground state back to itself via a virtual excited state. The effect of the first pulse can therefore be expressed as

$$|\mathbf{p}_0\rangle \overset{\text{Pulse}}{\rightarrow} |\psi(t=0+)\rangle=\sum_{n_1=-\infty}^{+\infty} c_{n_1}|\mathbf{p}_0+n_1\hbar\mathbf{q}\rangle, \qquad (1)$$

where the amplitudes c_{n_1} depend on the pulse area.

Immediately after the pulse, there is no atomic density modulation because the pulse is assumed to be sufficiently short so that the atoms do not have time to move during the pulse (this is the Raman-Nath approximation [22]). Although not obvious from Eq. (1), the wave function immediately after the pulse is modulated in *phase* with period $\lambda/2$ [see Sec. V, particularly Eq. (7)].

Owing to the dispersion of de Broglie waves in free space, the phase modulation immediately after the first pulse evolves into a density modulation (again, of period $\lambda/2$). Up to an overall phase, the state $|\psi(t=0+)\rangle$ changes in time as

$$|\psi(t)\rangle=\sum_{n_1=-\infty}^{+\infty} c_{n_1}e^{-in_1^2\omega_q t-in_1\mathbf{v}_0\cdot\mathbf{q}t}\ |\mathbf{p}_0+n_1\hbar\mathbf{q}\rangle, \qquad (2)$$

where $\mathbf{v}_0=\mathbf{p}_0/m_{\text{atom}}$ is the initial velocity of the atom, $n_1\mathbf{v}_0\cdot\mathbf{q}t$ is the Doppler phase, $\omega_q=\hbar\mathbf{q}^2/2m_{\text{atom}}$ is the recoil frequency, and $n_1^2\omega_q t$ is the recoil phase. (A stationary atom gains an energy of $\hbar\omega_q$ in a two-photon recoil.) The recoil frequency ω_q determines the time scale where quantum effects become significant. We define the Talbot time $T_q=2\pi/\omega_q\simeq 64$ μs for the Rb atoms in our experiment.

The atomic density $\rho_{\mathbf{v}_0}(x,t)$ from the initial momentum state $|\mathbf{p}_0\rangle$ can be computed from Eq. (2) by $\rho_{\mathbf{v}_0}(x,t)=|\langle\psi(t)|x\rangle|^2$. The total density is obtained by summing $\rho_{\mathbf{v}_0}(x,t)$ over the distribution of initial velocities $\mathbf{v}_0$. The modulation in the atomic density is due to the coherence between different momentum states. When summing over the initial velocity $\mathbf{v}_0$, this coherence is lost for sufficiently large time because the Doppler phases differ for different velocities. It can be seen from Eq. (2) that the time scale for this dephasing is of the order of $1/uq$ for a typical velocity spread u. In our experiments, this time is much less than the Talbot time.

After a single pulse, the overall period of the resulting atomic density modulation is $\lambda/2$. This modulation can be detected by switching on a weak readout field in the mode $\mathbf{k}_{\text{readout}}=\mathbf{k}_2$, as shown in Fig. 1(b). The atomic grating will backscatter the light into the mode $\mathbf{k}_1$ because of the phase-matching condition $\mathbf{k}_1=\mathbf{k}_{\text{readout}}-\mathbf{q}$. In our experiments, we measure the amplitude and phase of the backscattered field.

Although the period of the atomic density modulation is $\lambda/2$, the density distribution also contains higher spatial harmonics ($\lambda/4$, $\lambda/6$, etc.) because an atom could have received more than one recoil $\hbar\mathbf{q}$ from the standing-wave field. The goal of our experiment is to remove the lower spatial harmonics in the atomic density and end up with structures whose period is some integral fraction of $\lambda/2$. To achieve this goal, we rely on two phenomena: (i) the initial structure we created vanishes due to the thermal motion of atoms on the time scale $\lambda/2u\simeq 0.5$ μs, where u is the thermal velocity spread of the atomic cloud; (ii) by appropriate use of photon echoes, we can select out various spatial harmonics of the atomic density.

We now consider the effect on the atomic density of two standing-wave pulses separated by a time T_2. The behavior of the system can be clarified by use of a Doppler phase diagram [23], as shown in Fig. 2(a). This diagram plots the velocity-dependent phase of the atomic amplitudes that result from a sequence of optical pulses on an initial atomic state with velocity $\mathbf{v}_0$. As shown in Eq. (2), the first standing-wave pulse (SW1) produces a superposition of momentum states that differ from the initial momentum by multiples of $\hbar\mathbf{q}$. The amplitude of each of these states has a velocity-dependent phase $n_1\mathbf{v}_0\cdot\mathbf{q}t$ that increases linearly in time and is proportional to the number of recoils n_1. As the lines separate, the phase difference between interfering amplitudes de-

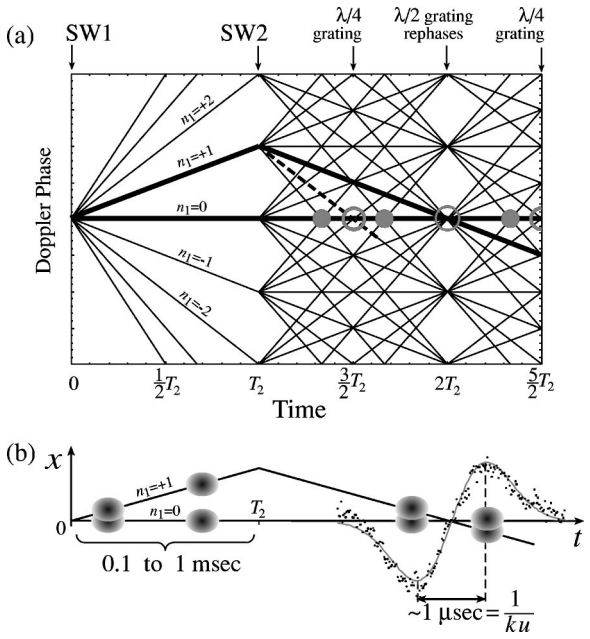

FIG. 2. Doppler phase diagram (or recoil diagram) for a two-pulse population grating echo experiment. n_1 is the number of two-photon recoils following the first pulse. (a) Possible trajectories of atomic amplitudes subject to two standing-wave pulses SW1 and SW2 (which are assumed to be short, and whose duration is not resolved in the plot). By solid lines, we have designated trajectories considered in part (b). The amplitude shown by the dashed trajectory produces a λ/4 period atomic grating at $t=\frac{3}{2}T_2$. Solid dots at $t=\frac{4}{3}T_2$, $t=\frac{5}{3}T_2$, and $t=\frac{7}{3}T_2$ show the instants when a grating of period λ/6 forms. (b) Billiard-ball model showing the interference of two wave packets that restore the initial λ/2 modulation. Around time $t=2T_2$, the experimental signal is shown.

pends on the initial atomic velocity, and any density grating produced is washed out in time $1/qu$ due to the spread in initial velocity. The second pulse (SW2) applied at time $t=T_2$ relative to the onset of SW1 ($T_2 \sim 0.1$–1 ms) further splits each of the amplitudes arising from the first pulse into a set of amplitudes. Crossing lines on this diagram represent the condition when the interference between states of different momentum does not depend on the atomic velocity, and a coherent atomic grating is produced. We refer to this revival of the initial modulation of the cloud as a *population grating echo*. The difference in slope between interfering amplitudes gives the periodicity of the resulting grating. For example, the solid thick lines in Fig. 2(a) represent interfering amplitudes that contribute to an echo at time $t=2T_2$. In this case the momentum state labeled $n_1=+1$ receives a momentum kick of $-2\hbar q$ from SW2 and crosses the momentum state $n_1=0$ at time $2T$. Because the difference in momentum between the interfering states is $\hbar q$, the periodicity of the resulting grating is λ/2. To compute the atomic density at $2T_2$ (or at any other echo time), one has to sum the contributions of all the interfering amplitudes that cross at this time.

Figure 2(a) is also referred to as a recoil diagram. According to the "billiard-ball echo model" [19], one can consider the initial state of the system as a wave-packet whose momentum spread is that of the entire gas. The laser pulse splits this wave packet into separate wave packets, which then separate over time as a result of the recoil momentum these wave packets receive from the light field. In Fig. 2(b), which shows this idea more graphically, we display the positions of only two wave packets that have received zero and one recoil, respectively. When these two wave packets are closer than the coherence length (thermal de Broglie wavelength), they interfere, and we observe modulation in the cloud. After their separation becomes larger, the modulation washes out. The second pulse creates a wave packet from the $n_1=+1$ wave packet that propagates back toward the $n_1=0$ wave packet and overlaps it at time $2T_2$, producing a density grating in the vicinity of the time $2T_2$.

We can detect the restored modulation by means of scattering a weak readout wave. The amplitude of the signal backscattered around $t=2T_2$ is shown in Fig. 2(b) [see also Fig. 6]. At exactly $t=2T_2$ this signal is zero (no scattering) because the density is uniform at this instant (as in the situation immediately after the first pulse—see Sec. V).

The structure of period λ/2 appearing around $t=2T_2$ has been studied in Ref. [24]. The focus of this paper is on producing density modulations of smaller period. Such gratings will form in response to two pulses at times other than integer multiples of T_2. An example of this is shown by the dashed line in Fig. 2(a). This line is formed by the amplitude that picked up momentum $\hbar\mathbf{q}$ from the first pulse (labeled $n_1=1$) receiving a momentum kick from the second pulse of $-3\hbar\mathbf{q}$ (as opposed to $-2\hbar\mathbf{q}$ for the echo that occurs at $t=2T_2$). This line crosses the horizontal axis, which represents an amplitude with initial momentum $\mathbf{p}_0$, at $t=(3/2)T_2$ with a slope of $-2\hbar\mathbf{q}$, resulting in a grating with a period of λ/4 because (i) the difference in momenta of the interfering amplitudes is $2\hbar\mathbf{q}=4\hbar\mathbf{k}$, and (ii) no amplitudes with momentum difference of $\hbar\mathbf{q}$ interfere at this time and therefore the density harmonic of period λ/2 is absent. In a similar fashion we expect to get a periodicity of λ/6 around $t=(4/3)T_2$ because the minimum difference between the momenta of interfering states is $3\hbar\mathbf{q}$. Around $t=\frac{5}{4}T_2$, we have a grating of period λ/8 and so on.

The structures of period smaller than λ/2 do not scatter the wave $\mathbf{k}_2$. We detect these structures indirectly by applying the third standing-wave pulse (SW3) at $t=T_3$ whose effect is displayed in Fig. 3. SW3 converts interfering amplitudes with a large difference in momentum recoils (which are capable of producing gratings of period smaller than λ/2) into amplitudes that differ by only one recoil, and therefore produce a structure with λ/2 period that can be detected directly. The thick lines in Fig. 3 show an example of a grating of period λ/4 at time $3T/2$ that is converted by SW3 into a λ/2 grating that appears at a later time. Listed also in this figure (in rectangular boxes) is the difference in momentum in numbers of recoils (symbolized by integers N_1, N_2, and N_3) after each pulse for the amplitudes represented by the thick lines. The signal from this λ/2 structure (*the echo*) contains information about the previously existing smaller period density gratings. The properties of the three-pulse echo shown in Fig. 3 depend on the coherence between states differing by a particular value of N. The existence of this

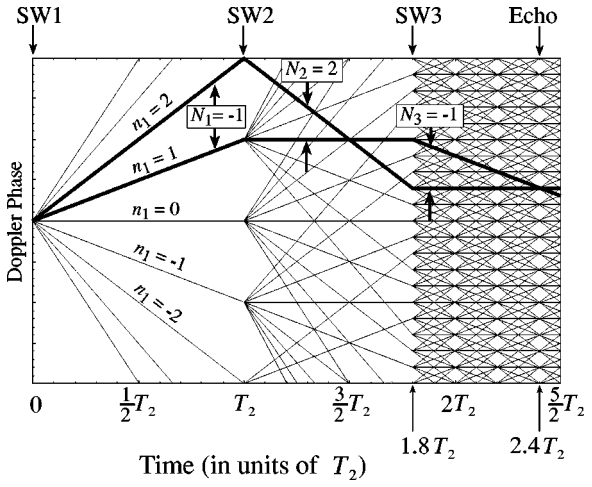

FIG. 3. Doppler phase diagram showing detection of higher-order gratings for a particular onset time of SW3: $T_3 = 1.8T_2$. The third standing-wave pulse (SW3) converts amplitude differences that produce a higher-order structure into the ones that give a structure of period $\lambda/2$, detectable directly. The N_1, N_2, and N_3 refer to differences in momentum of interfering amplitudes in units of $\hbar q$.

echo is direct evidence of the existence of this coherence, and in addition, gives information about the size of this coherence. While the three-pulse echo signal is not a direct indicator of the existence of the higher-order echo (it can even occur before the higher echo occurs as in the case of the ''slow'' echo described later), it indicates the presence of the coherences that result in the higher-order echo. Measurement of the three-pulse signal as a function of various parameters (e.g., time between pulses) and comparison of the results to the detailed theory (developed in Sec. V) allows one to obtain specific information, such as contrast, about the high-order echo.

The Doppler phase diagrams representing the echoes that occur as a result of a sequence of pulses can be simplified by realizing that the time a given echo occurs is uniquely determined by the momentum difference in interfering amplitudes after each of the standing-wave pulses. A plot of the Doppler phase *difference* between pairs of interfering amplitudes produces a significantly simpler diagram that clearly indicates the relationship between the values of N_j, the pulse times T_j, and the time of the echo. Figure 4(a) shows such a diagram representing the equivalent situation as the thick lines in Fig. 3. In this diagram, the slope of the Doppler phase difference is proportional to the value of N_j, and an echo occurs with spatial period $\lambda/(2N_j)$ when the Doppler phase difference crosses zero with slope corresponding to momentum difference $N_j\hbar\mathbf{q}$.

In our experiment, we have observed three kinds of echo, distinguished experimentally by the different dependence of the echo time on the onset times of the SW pulses. Figure 4 shows the phase diagrams that lead to each of these echoes. The atoms as displayed in Figs. 4(a) and 4(b) would have produced a $\lambda/4$ grating at $t = \frac{3}{2}T_2$ if SW3 were not applied. We shall call the echoes, described in Figs. 4(a) and 4(b), the ''fast'' and the ''slow'' echo, respectively. These echoes are named because of the different dependence of t^{echo} on the

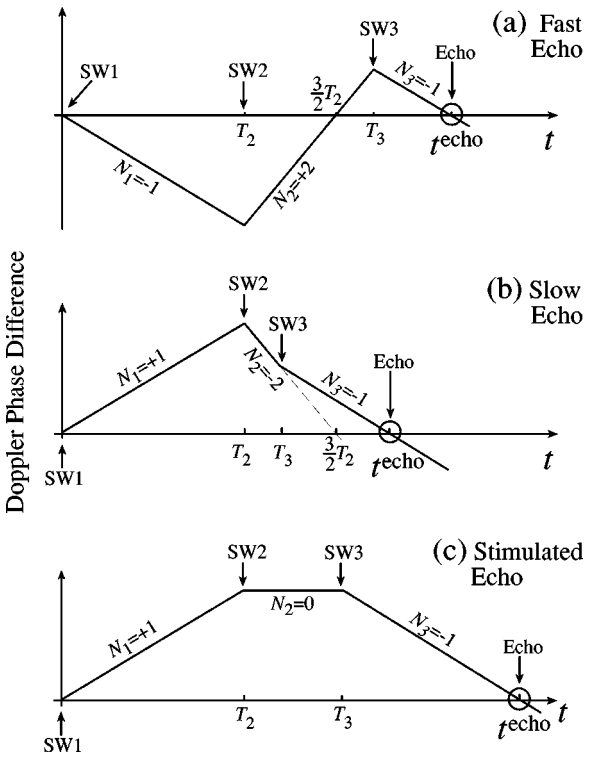

FIG. 4. Phase diagrams for (a) fast echo, (b) slow echo, and (c) stimulated echo.

onset of SW3. The times when the echoes occur are

$$t_{\text{fast}}^{\text{echo}} = -3T_2 + 3T_3, \tag{3a}$$

$$t_{\text{slow}}^{\text{echo}} = 3T_2 - T_3. \tag{3b}$$

From these equations it is clear that when T_3 is changed, $t_{\text{fast}}^{\text{echo}}$ changes three times more than $t_{\text{slow}}^{\text{echo}}$.

We also studied another kind of echo that we call the ''stimulated'' echo in analogy to the stimulated photon echo [25] [see the diagram in Fig. 4(c)]. In contrast to the slow and the fast echo, the stimulated echo does not involve the formation of structures smaller than $\lambda/2$. That is, it does not involve coherences between atomic amplitudes with $|N_j| > 1$, and no higher-order atomic grating would form if the third pulse were not applied. It is still a three-pulse echo, however, in that it does not exist if one of the pulses is not applied. The stimulated echo can be observed at

$$t_{\text{stim}}^{\text{echo}} = T_2 + T_3. \tag{4}$$

We note that the echo phenomenon itself—that is, the rephasing of the atomic density gratings at various echo times—does not depend on the quantization of the atomic center of mass. For example, a gas of classical particles subject to a sequence of transmission gratings (array of thin slits) would result in the rephasing of gratings of various periodicities at the same echo times as for the experiments discussed in this paper [21,26,27]. The size (or contrast) of the gratings produced, on the other hand, depends specifically on the mechanism that produces these gratings. For the

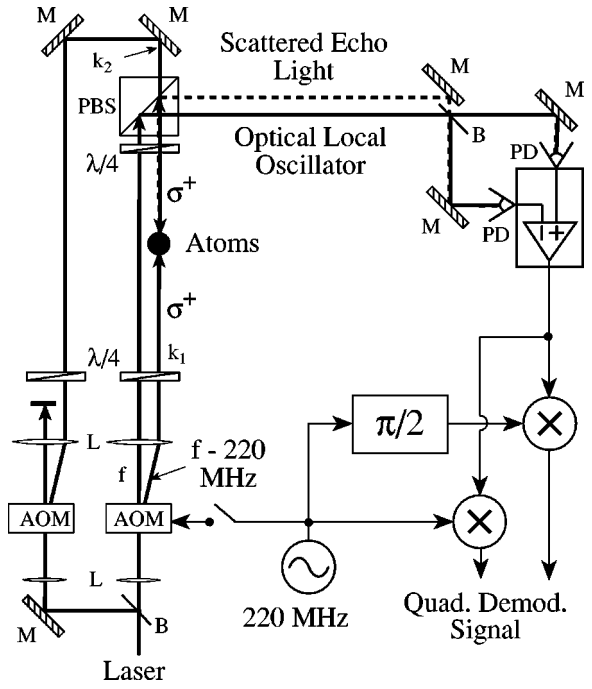

FIG. 5. Schematic diagram of the experimental setup. M=mirror, B=beam splitter, PD=photodiode, AOM=acousto-optic modulator, $\lambda/2$=half-wave plate, $\lambda/4$=quarter-wave plate, L=lens, PBS=polarizing beam splitter, and $\otimes$=mixer. $f=c/\lambda=3.8\times10^{14}$ Hz is the laser frequency.

system discussed in this paper, this size depends strongly on the recoil phase of the various amplitudes contributing to the echo, and therefore depends in a critical way on the quantum nature of the center-of-mass motion. As shown in Secs. IV and V, the size of the echo signal (which is proportional to the grating contrast) as a function of the onset time of the standing-wave pulses is strongly modulated at multiples of the recoil frequency ω_q. This modulation is closely related to the atomic Talbot effect [28,29].

III. EXPERIMENTAL SETUP

The experimental setup is similar to the interferometer of Cahn *et al.* [24] and is shown in Fig. 5. Our experiment is repeated every 100 ms. Each duty cycle consists of a trapping and cooling period (88 ms) and an experimental period (within the next 12 ms). During the trapping and cooling period we prepare a cold atomic sample for the interferometer. This is done in two steps. During the first 80 ms, we cool and trap ^{85}Rb in the vapor-cell magneto-optical trap [30]. The trapping laser is detuned by 3Γ from the transition $5S_{1/2}(F=2)\rightarrow5P_{3/2}(F'=4)$, where Γ is the natural linewidth of the excited level. Then we turn off the trapping magnetic field, detune the laser up to 6Γ to the red of the resonance, and further cool atoms in optical molasses via polarization gradient cooling [31,32] for 7.9 ms. As a result, we get a cloud of atoms at 105 μK. For trapping and cooling we use a diode laser system that is independent of a Ti:sapphire laser used to produce beams $\mathbf{k}_1$ and $\mathbf{k}_2$.

The beginning of the experimental cycle (0.1 ms after the molasses beams are switched off) is referred to as time $t=0$. At $t=0$, $t=T_2$, and $t=T_3$ three off-resonant standing-wave pulses (SW1, SW2, and SW3) are applied with pulse durations of 50 ns. The pulses are 434 MHz ($\simeq$80 excited-state linewidths) blue shifted from the closest transition $5S_{1/2}(F=3)\rightarrow5P_{3/2}(F'=4)$ of ^{85}Rb. This large detuning allows us to minimize the effects of spontaneous emission (we estimate that less than 1% of the atoms spontaneously emit during each pulse). The SW pulses are composed of two counterpropagating traveling waves $\mathbf{k}_1$ and $\mathbf{k}_2$, switched on and off independently by two acousto-optic modulators (AOM). The AOMs are driven by a common 220-MHz rf oscillator. The density grating of the atomic cloud is probed by switching on only the traveling wave along $\mathbf{k}_2$ and measuring the (complex) amplitude of the wave backscattered along $\mathbf{k}_1$. For the SW pulses, the power in each $\mathbf{k}_1$ and $\mathbf{k}_2$ beam is 115 mW and the intensity is approximately 460 mW/cm^2, while the intensity of the probe beam is 15 times smaller. Typical pulse areas [see Eq. (7)] used in our experiments ranged from about 1.5 to 2.

The scattered wave is detected by beating it with an optical local oscillator in a balanced heterodyne arrangement. The optical local oscillator is the beam passing undiffracted through the AOM used to switch the $\mathbf{k}_1$ beam. The echo beat signal (at 220 MHz) obtained from the heterodyne arrangement is mixed down to dc in a quadrature demodulator. The two outputs of the demodulator are the real and imaginary part of the scattered light amplitude.

To compensate for drifts in the phase between repetitions of the experiment (due, for example, to motion of the mirrors), the following phase stabilization scheme was used [33]. Before each repetition of the experiment a weak rf signal was applied to the $\mathbf{k}_1$ AOM, resulting in a weak optical signal along the $\mathbf{k}_1$ direction. A feedback loop was used to adjust the phase of the rf signal until the output of one channel of the demodulated beat signal between the $\mathbf{k}_1$ beam and the optical local oscillator was reduced to zero. This phase was then held fixed during the subsequent pulse sequence leading to the echo signal. Therefore, the real and imaginary parts of the complex echo signal represent the components of the signal field in phase and in quadrature with the applied $\mathbf{k}_1$ field, respectively (note that the $\mathbf{k}_1$ field is off during the detection). Any phase drift during a single repetition of the experiment was minimized by directing the optical local oscillator and the $\mathbf{k}_1$ beam through the same set of optics (see Fig. 5).

IV. EXPERIMENTAL RESULTS

In Fig. 6, we have plotted a typical echo signal from the experiment. The amplitude of the scattered light is plotted as a function of the time Δt relative to the calculated echo time t^{echo}. The dots are the experimental data and the curve is a fit to the theoretical prediction (17), which will be derived later. Though we measure both real and imaginary part of the electric-field amplitude, only one trace is displayed in Fig. 6. This is because the real and imaginary parts of the data are proportional to each other, and a time-independent rotation in the complex plane during the data analysis can be used to

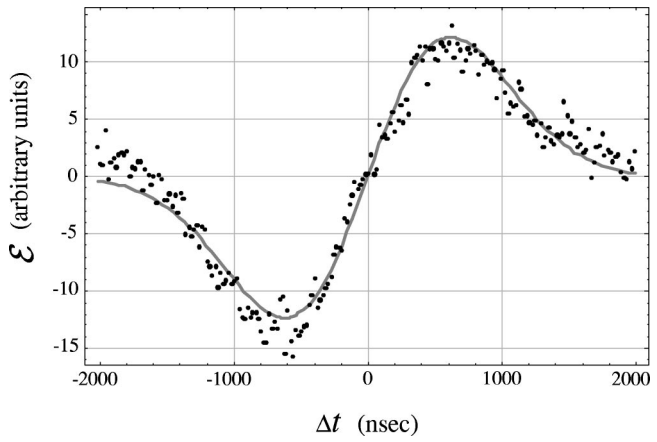

FIG. 6. A typical echo signal: the amplitude of the backscattered light vs time $\Delta t \equiv t - t^{\text{echo}}$. Dots are the data, and the curve is the fit to the theory [Eq. (17)].

reduce one component of the signal to nearly zero. Figure 6 shows only the nonzero component of the rotated signal. A negative value of $\mathcal{E}$ in Fig. 6 (occurring at times $\Delta t < 0$) corresponds to a grating that is shifted by half a grating period from a grating that produces a positive value of $\mathcal{E}$ (occurring at times $\Delta t > 0$ in Fig. 6).

One may see in Fig. 6 that no light is scattered from the

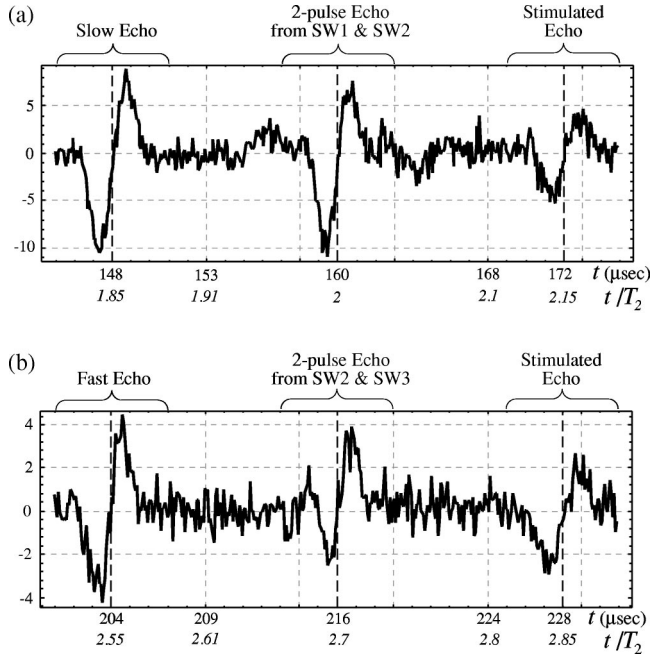

FIG. 7. Data showing the backscattered echo signals vs time: (a) $T_2 = 80$ μs and $T_3 = 92$ μs. On this trace, the slow echo, the two-pulse echo from SW1 and SW2, and the stimulated echo are displayed. While the echoes on the left and right require all three standing-wave pulses for their generation, the echo in the middle needs only SW1 and SW2. (b) $T_2 = 80$ μs and $T_3 = 148$ μs. This trace displays the fast echo, the two-pulse echo from SW2 and SW3, and the stimulated echo. The echo in the middle requires only SW2 and SW3 for its generation. Recoil diagrams for the slow, fast, and stimulated echoes are shown in Fig. 4.

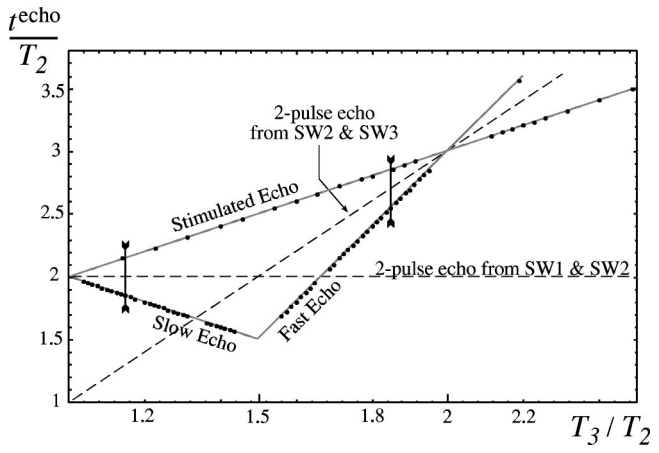

FIG. 8. The echo time vs the onset of the third pulse. Both the echo time and the position of the third pulse are normalized to T_2. Dots are the data and the lines are the theory [Eqs. (3) and (4)]. For the slow and fast echo, T_2 was fixed at 80 μs; for the stimulated echo, $T_2 = 35$ μs. The two vertical segments at $T_3/T_2 = 1.15$ and at $T_3/T_2 = 1.85$ show the time intervals covered by the traces of Fig. 7.

atomic cloud at time $\Delta t = 0$. This is because there is no modulation in density at this instant. It is a remarkable fact that for any sequence of standing-wave pulses, the modulation in atomic density is zero at exactly the echo times. This is due to cancellation of the recoil phases of the amplitudes contributing to the echo signal at the same instant that the Doppler phases cancel. See Sec. V for further discussion of this point. The amplitude of the scattered light increases immediately after the point $\Delta t = 0$ as the density grating forms, and then drops off because of the thermal motion of the atoms. The opposite order of evolution is seen when the time is approaching the instant $\Delta t = 0$. The temporal width of the signal is an accurate measure of temperature, which was found to be $T = 105$ μK, corresponding to the thermal velocity $u = 14$ cm/s ($u = \sqrt{2k_B T/m_{\text{atom}}}$). In general, one can extract the entire velocity distribution (projected along the direction of **q**) from the shape of the echo signal.

At certain onset times of the pulses, echoes of different kinds appear close enough to each other that one can see them on the same trace on the oscilloscope. Two such traces are displayed in Fig. 7. The slow and the stimulated echoes are plotted in Fig. 7(a) (the echo in the middle is the two-pulse echo from SW1 and SW2, it remains there if SW3 is not applied); the fast and the stimulated echo are displayed in Fig. 7(b) (again the echo in the middle is a two-pulse echo, now from SW2 and SW3).

In our experiments, we fixed the onset times of SW1 and SW2 and varied the time at which SW3 is applied. Figure 8 shows the dependence of the echo time on the onset time of the third pulse: Both the data and the theoretical predictions of Eqs. (3) and (4) are plotted. It is interesting to see in Fig. 8 that the slow echo moves backwards with increasing T_3, while the times when the fast and the stimulated echo occur increase. The positions of the two traces of Fig. 7 are shown by two vertical segments.

An important parameter that determines contrast of the

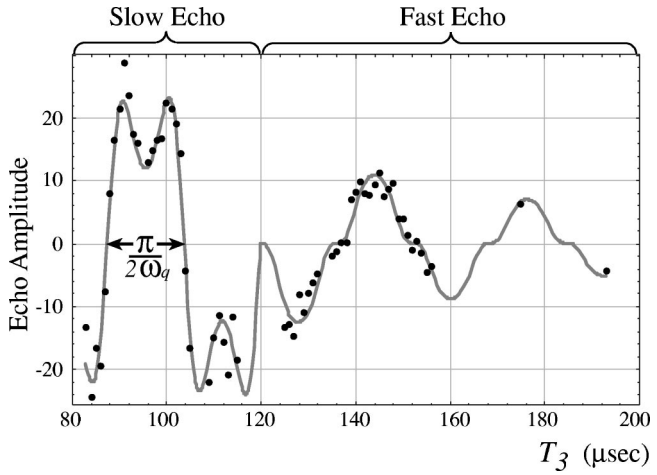

FIG. 9. Amplitude of the slow and fast echo vs onset time of the third standing-wave pulse, T_3, with T_2 fixed at 80 μs. The oscillations in the signal amplitude are composed of harmonics of $2\omega_q$. When T_3 goes over the point $T_3=1.5T_2$, we stop seeing the slow echo and see, instead, the fast echo. Dots are experimental points and the solid line is a fit based on Eq. (24) multiplied by a phenomenological decay factor $\exp[-(t^{\text{echo}}/320\ \mu\text{s})^2]$.

fabricated structures and the size of the echo signal is the recoil phase. To see the influence of the recoil phase on the echo signal, we measured the dependence of the echo peak-to-peak size on the onset time of SW3 (T_3), keeping the onset time of SW2 (T_2) constant. Figure 9 shows this dependence for the slow and fast echo. The dots are the experimental data and the curve is the theory [based on Eq. (24)]. Each point on this graph is a result of a separate experiment in which a trace similar to the one of Fig. 6 is observed and the echo peak-to-peak size entered into the graph of Fig. 9. One may see that the echo size oscillates on the time scale of $\pi/\omega_q \simeq 32\ \mu$s. By a proper choice of the recoil phase, one may achieve maximum visibility in the desired periodic structure.

In addition to the oscillations in the echo size as a function of the pulse times T_j, we find that there is an overall decay of the size of the echo as the echo time t^{echo} increases. We have measured echo lifetimes (the value of t^{echo} where the echo signal is e^{-1} its maximum size) as long as 2.0 ms. In principle, the echo lifetime should be determined only by how long the atoms remain in the interaction region, and for the parameters of our experiment, we estimate this time to be on the order of 10 ms. The reason for this discrepancy has not been unambiguously determined. The echo lifetime for the data in Fig. 9 was about 300 μs, which we found to be due to a small amount of resonant light that was continuously irradiating the atoms during the experiment.

We note here that one would expect a large number of different three-pulse echos, corresponding to different values of N_1 and N_2 (see Fig. 4). In addition to the echos shown in Fig. 4, we have observed a three-pulse echo corresponding to the formation of a $\lambda/6$ grating at time $t=(4/3)T$. Other echos should be easily observed with our apparatus by using the results of Sec. V to determine the optimum parameters for a given echo. Up till now, however, no systematic search has been carried out.

V. THEORETICAL ANALYSIS

A. Periodic structures in a gas of two-level atoms

So far the underlying physics has been described qualitatively. We now study quantitatively the effect of a sequence of standing-wave pulses on a sample of cold atoms. In this section, we shall study the formation of periodic structures in a gas of two-level atoms. In fact, the experiment has been done in a gas of ^{85}Rb atoms whose ground and excited states have a hyperfine structure. Our theoretical results will be generalized to multilevel atoms in Sec. V B.

For the purpose of quantitative analysis, we model the gas of atoms as an incoherent Maxwell-Boltzmann mixture of plane waves. We carry out the calculation by first computing the signal for a well-defined initial momentum $\mathbf{p}_0=m\mathbf{v}_0=\hbar\mathbf{q}_0$ and then summing the signal over the initial atomic momentum distribution. We assume that the detuning $\Delta \equiv \omega_{\text{laser}}-\omega_{eg}$ is sufficiently large so that the atom always remains in the ground state and spontaneous emission can be neglected. The Rabi frequency will be defined via the (real) electric-field amplitude $\mathcal{E}_0$ and polarization $\boldsymbol{\sigma}$ of traveling waves forming the standing-wave field:

$$\hbar\chi \equiv |-\mathbf{d}_{eg}\cdot\boldsymbol{\sigma}\mathcal{E}_0|, \tag{5}$$

where $\mathbf{d}_{eg}$ is the dipole matrix element connecting the excited and the ground state.

Under the above conditions, the ground state of an atom placed into a standing-wave field shifts [22,34] up to a constant term as

$$V(\mathbf{x},t)=\hbar\Omega(t)\cos(\mathbf{q}\cdot\mathbf{x}), \tag{6}$$

where $\Omega(t)=[\chi(t)]^2/(2\Delta)$ is the two-photon Rabi frequency. This spatially varying energy shift determines the motion of the atoms.

To see the effect of the first standing-wave pulse on an initial atomic plane wave $\exp(i\mathbf{q}_0\cdot\mathbf{x})$ and find the wave function after the pulse, $\psi(\mathbf{x},t=0+)$, we apply time evolution operator $\exp[-i\int\hat{H}(t)dt/\hbar]$. During the pulse, we neglect the kinetic-energy term $\hat{\mathbf{p}}^2/2m$ in the Hamiltonian (Raman-Nath approximation [22]). This approximation, which is based on the assumption that the atoms do not move during the interaction is valid when $qu\tau \ll 1$, $\omega_q\tau \ll 1$, and $\sqrt{\omega_q\Omega}\ \tau \ll 1$ for pulse duration τ. Therefore, during the pulse, $\hat{H}(t)=V(\mathbf{x},t)$, and the wave function after the first pulse is

$$\psi_{\mathbf{v}_0}(\mathbf{x},t=0+)=e^{i\theta_1\cos(\mathbf{q}\cdot\mathbf{x})}e^{i\mathbf{q}_0\cdot x}, \tag{7}$$

where $\theta_j=-\int\Omega(t)dt$ is the pulse area. As it is seen from Eq. (7), the pulse does not alter the density distribution $(|\psi_{\mathbf{v}_0}(\mathbf{x},0+)|^2=1)$ but imposes a periodic phase modulation of period $\lambda/2$. A Fourier transform shows that Eq. (7) is a superposition of partial plane waves whose momenta differ by the multiples of the recoil momentum $\hbar\mathbf{q}$:

$$\psi_{\mathbf{v}_0}(\mathbf{x},t=0+)=\sum_{n_1=-\infty}^{+\infty} i^{n_1}J_{n_1}(\theta_1)e^{i(\mathbf{q_0}+n_1\mathbf{q})\cdot\mathbf{x}}, \tag{8}$$

where J_{n_1} is a Bessel function of the first kind.

Between pulses, the evolution of the atomic state is determined by the free particle Hamiltonian $\hat{H}=\hat{\mathbf{p}}^2/2m_{\text{atom}}$. Up to an overall phase (which is unimportant for interference) the wave function is

$$\psi_{\mathbf{v}_0}(\mathbf{x},t)=\sum_{n_1=-\infty}^{+\infty} i^{n_1}J_{n_1}(\theta_1)e^{-in_1\mathbf{v}_0\cdot\mathbf{q}t-in_1^2\omega_q t}e^{i(\mathbf{q}_0+n_1\mathbf{q})\cdot\mathbf{x}}. \tag{9}$$

Equations (8) and (9) are essentially the same as Eqs. (1) and (2), but written in a different representation. The Doppler phase $n_1\mathbf{v}_0\cdot\mathbf{q}t$ is responsible for rapid loss of coherence between classes of atoms with different initial velocities. The recoil phase $n_1^2\omega_q t$ varies much more slowly.

To see the effect of a sequence of L short standing-wave pulses on an atom plane wave, one should apply a sequence of time evolution operators: $\exp[i\theta_j\cos(\mathbf{q}\cdot\mathbf{x})]=\Sigma_{n_j}i^{n_j}J_{n_j}(\theta_j)e^{in_j\mathbf{q}\cdot\mathbf{x}}$ for each (jth) pulse with onset time T_j, and $\exp[-i\hat{\mathbf{p}}^2(t-T_j)/2\hbar m_{\text{atom}}]$ for the interval of free evolution before the next pulse or the detection. Each pulse splits partial waves as the first pulse splits the initial state. At some time t after L pulses, the wave function is

$$\begin{aligned}\psi_{\mathbf{v}_0}(\mathbf{x},t)=&\sum_{n_1\ldots n_L=-\infty}^{+\infty} i^{n_1+\cdots+n_L}J_{n_1}(\theta_1)\cdots J_{n_L}(\theta_L)\\&\times\exp\{-i\mathbf{v}_0\cdot\mathbf{q}[n_1(T_2-T_1)+(n_1+n_2)(T_3-T_2)\\&+\cdots+(n_1+\cdots+n_{L-1})(T_L-T_{L-1})\\&+(n_1+\cdots+n_L)(t-T_L)]\}\\&\times\exp\{-i\omega_q[n_1^2(T_2-T_1)+(n_1+n_2)^2(T_3-T_2)\\&+\cdots+(n_1+\cdots+n_{L-1})^2(T_L-T_{L-1})\\&+(n_1+\cdots+n_L)^2(t-T_L)]\}e^{i[\mathbf{q}_0+(n_1+\cdots+n_L)\mathbf{q}]\cdot\mathbf{x}}.\end{aligned} \tag{10}$$

To find the density of atoms corresponding to the above wave function, we average $|\psi_{\mathbf{v}_0}(\mathbf{x},t)|^2$ over the initial velocity distribution $f(\mathbf{v}_0)$. We write the resulting density as Fourier series

$$\rho(\mathbf{x},t)=\sum_{N_L=-\infty}^{+\infty}\rho_{N_L}(t)e^{iN_L\mathbf{q}\cdot\mathbf{x}}, \tag{11}$$

where the N_Lth Fourier harmonic is built up by interfering matter waves whose momenta differ by N_L recoils (that is, $N_L\hbar\mathbf{q}$). The amplitude of the N_Lth Fourier harmonic of density is [35]

$$\begin{aligned}\rho_{N_L}(t)=&\sum_{N_1\cdots N_{L-1}=-\infty}^{+\infty}\langle e^{-i\mathbf{v}_0\cdot\mathbf{q}N_L(t-t_{\mathbf{N}}^{\text{echo}})}\rangle_f\\&\times J_{N_1}(2\theta_1\sin\varphi_1^{\text{rec}}(t))\\&\times\prod_{j=2}^{L}J_{N_j-N_{j-1}}(2\theta_j\sin\varphi_j^{\text{rec}}(t)),\end{aligned} \tag{12}$$

where $\langle\cdots\rangle_f$ designates averaging over the initial velocity distribution, the time

$$t_{\mathbf{N}}^{\text{echo}}=T_L-\frac{1}{N_L}\sum_{j=1}^{L-1}N_j(T_{j+1}-T_j) \tag{13}$$

is the echo time for a given value of $\mathbf{N}\equiv\{N_1,\ldots,N_L\}$ (represented by $\mathbf{N}$ in $t_{\mathbf{N}}^{\text{echo}}$), and the phases

$$\begin{aligned}\varphi_j^{\text{rec}}(t)=&\omega_q\left[N_L(t-T_L)+\sum_{l=j}^{L-1}N_l(T_{l+1}-T_l)\right]\\&(j=1,\ldots,L-1),\\\varphi_L^{\text{rec}}(t)=&\omega_q N_L(t-T_L)\end{aligned} \tag{14}$$

arise from the recoil phases of interfering waves and are responsible for the slow oscillations of the echo amplitude as a function of pulse times T_j.

It is clear from Eq. (13) that the echo time only depends on the onset time of the pulses and on the differences in recoil momenta of interfering waves after each pulse. Equations (3) and (4), giving the instant of the slow, fast, and stimulated echo are particular cases of Eq. (13).

Because of the thermal velocity spread, the factor $\langle e^{-i\mathbf{v}_0\cdot\mathbf{q}N_L(t-t_{\mathbf{N}}^{\text{echo}})}\rangle_f$ in Eq. (12) differs from zero only when $|t-t_{\mathbf{N}}^{\text{echo}}|\leqslant 1/N_L qu$ (Doppler dephasing time). Thus, we need to only consider the signal for times $t=t_{\mathbf{N}}^{\text{echo}}+\Delta t$, where $|\Delta t|\leqslant 1/N_L qu$. We have, for a given value of $\mathbf{N}$, and for the particular case of a Maxwell velocity distribution, $f(\mathbf{v}_0)=\exp(-v_0^2/u^2)$,

$$\begin{aligned}\rho_{N_L}(t)=&e^{-(N_L qu\Delta t/2)^2}J_{N_1}(2\theta_1\sin(N_L\omega_q\Delta t))\\&\times\prod_{j=2}^{L}J_{N_j-N_{j-1}}(2\theta_j\sin[\varphi_j^{\text{rec}}(t_{\mathbf{N}}^{\text{echo}}+\Delta t)]),\end{aligned} \tag{15}$$

where we have used in the argument of J_{N_1} the fact that $\varphi_1^{\text{rec}}(t_{\mathbf{N}}^{\text{echo}}+\Delta t)=N_L\omega_q\Delta t$ from Eqs. (13) and (14). Because $J_{N_1}(0)=0$ (for $N_1\neq 0$), we arrive at the remarkable result that the density modulation is zero at the exact echo times $\Delta t=0$.

Since in our detection scheme only $\lambda/2$ gratings scatter light effectively, the amplitude of scattered readout light is proportional to the weight of the minus-first Fourier harmonic of density ($N_L=-1$):

$$\mathcal{E}\propto\mathcal{E}_0\rho_{-1}(t), \tag{16}$$

TABLE I. Maximum visibility $V_{\max}$ for various values of N and the value of the pulse area θ_2 required to achieve this visibility.

N	$V_{\max}$ (%)	θ_2
1	57	1.5
2	51	2.1
3	47	2.6
4	44	3.2
10	34	6.4
15	30	9.0
20	28	11.6

where $\mathcal{E}_0$ is the amplitude of the readout field. To find the shape of the observed echo signal, we express the amplitude of this harmonic [ρ_{-1} given by Eq. (15)] to lowest order in Δt:

$$\mathcal{E} \propto \mathcal{A}(\Delta t)^{|N_1|} e^{-(qu\Delta t/2)^2}. \tag{17}$$

In this expression, $(\Delta t)^{|N_1|}$ appears from expanding $J_{N_1}(2\theta_1 \sin(N_L \omega_q \Delta t))$ with $N_L = -1$ in Eq. (15). The form (17) is consistent with the echo signals shown in Figs. 6 and 7 (where $N_1 = \pm 1$). The amplitude of the echo $\mathcal{A}$ varies as a function of the T_j on a relatively slow time scale of π/ω_q and is roughly independent of Δt:

$$\mathcal{A} \approx \prod_{j=2}^{L} J_{N_j - N_{j-1}}(2\theta_j \sin \varphi_j^{\mathrm{rec}}(t_{\mathbf{N}}^{\mathrm{echo}})). \tag{18}$$

The T_j's are assumed to be much larger than $1/qu$.

It is clear from Eq. (17) that the echo signal as a function of Δt allows one to determine u, which is the velocity spread of the atomic cloud projected along the direction of **q**. For $N_1 = 1$, for example, the maximum of the signal occurs at $\Delta t = qu$. Thus, from the shape of the observed signal, we can deduce the temperature of our trapped atoms.

It is interesting to calculate the maximum visibility, or contrast, of the atomic gratings produced by the techniques discussed in this paper. For this purpose, we consider a two-pulse experiment ($L = 2$) with pulses at times $T_1 = 0$ and T_2, and with $N_1 = -1$, and $N_2 = N$. Equation (13) gives the echo times $t = [1 + (1/N)]T_2$ for structures of period $\lambda/(2N)$ [see also, Fig. 2(a)]. Inserting these conditions into Eq. (15) yields

$$\rho_N(t) \approx e^{-(Nqu\Delta t/2)^2} J_1(2\theta_1 \sin(N\omega_q \Delta t)) \times J_{N+1}(2\theta_2 \sin(\omega_q T_2)). \tag{19}$$

Since ρ_0 is the total atomic density [see Eq. (11)], and in the vicinity of any given echo time, one particular value of N predominates, the visibility of the resulting atomic density— defined as $V \equiv (\rho_{\max} - \rho_{\min})/(\rho_{\max} + \rho_{\min})$, where $\rho_{\min}$ ($\rho_{\max}$) is the minimum (maximum) of ρ as a function of position— is given by $V = 2\rho_N$. The maximum visibility that can be obtained, $V_{\max}$, is twice the maximum of $J_1 J_{N+1}$ [see Eq. (19)]. These maximum visibilities for various N are listed in Table I. The maximum of $J_{N+1}(2\theta_2 \sin(\omega_q T_2))$ can be achieved by setting $\omega_q T_2 = \pi/2$ (or an odd multiple of $\pi/2$), and using values of θ_2 given in Table I. The optimum value of θ_1 depends on the Doppler width qu of the atomic cloud. One finds roughly that one can approach the maximum value $V_{\max}$ for $\theta_1 \geqslant qu/\omega_q$. For the atomic cloud used in our experiments, Eq. (19) indicates that for $\theta_1 = 10$, we can achieve a visibility of $0.54 V_{\max}$, $\theta_1 = 20$ gives $0.80 V_{\max}$ and $\theta_1 = 30$ gives $0.90 V_{\max}$. Colder atoms would achieve such visibilities with smaller θ_1.

It is worthwhile stressing that Eq. (12) was derived under the Raman-Nath assumption. This assumption becomes increasingly difficult to satisfy as the pulse angles θ_j get larger.

The results of this section can also be applied to the case of an atomic beam passing through spatially separated interaction regions. Such a configuration would be necessary for any deposition of atoms onto a surface. As mentioned in the Introduction, since the technique is based on echoes, no subrecoil collimation of the atoms being deposited is needed, potentially allowing a significantly higher atomic flux compared to techniques that require subrecoil collimation (such as those based on the Talbot effect). The question arises as to what degree a spread in *longitudinal* velocity one may have without significantly degrading the contrast of the resulting structures.

For sufficiently high longitudinal velocity v, one may substitute $z = vt$, where z is the position along the direction of the atomic beam. Atoms with different longitudinal velocity will therefore experience different interaction times with the fields resulting in a spread in pulse angles. In addition, the free evolution (fe) time between interaction zones, $T_{\mathrm{fe}} = D/v$, where D is the spacing between zones, depends on atomic velocity. Because the echo time is proportional to the free evolution time between fields, the spatial location of the echo will not depend on velocity. However, an averaging of the signal over longitudinal atomic velocity may reduce the contrast of the atomic fringes. Numerical calculations for the two-pulse experiment discussed above indicates that a longitudinal velocity spread ($v_{\max}/v_{\min}$) of up to a factor of 2 will not significantly degrade the contrast of the resulting density grating.

B. Generalization for multilevel atoms

Equation (15) expressing the size of the atomic density gratings has been derived in the case of two-level atoms. Our experiments were performed with Rb atoms, which have a multilevel structure. By optical pumping before the experiment and by use of appropriately polarized laser fields during the experiment, Rb can be effectively reduced to a two-level system. In the experiments described in this paper, however, no optical pumping was performed. In this section, we show how the results of the preceding section can be generalized to the case of a multilevel atom.

There are two aspects to this generalization. One is that a given ground-state sublevel is coupled to more than one excited state by the standing-wave pulses. The other is that if more than one ground-state sublevel is initially populated, then the total signal is the sum of the contributions from each of these sublevels. In the derivation that follows, we assume

that all ground-state sublevels contributing to the atomic density have equal populations.

To take into account multiple excited-state levels, one replaces Eq. (6) with

$$V_g(\mathbf{x}) = \hbar \Omega_g(t) \cos(\mathbf{q}\cdot\mathbf{x}), \tag{20}$$

where

$$\Omega_g = \sum_e \frac{\chi_{eg}^2}{2\Delta_{eg}}, \tag{21}$$

χ_{eg}^2 [given by Eq. (5)] is the Rabi frequency for the transition between a given ground state (labeled g) and excited state (labeled e), and Δ_{eg} is the detuning between the laser field and the transition frequency between g and e. For a given ground-state sublevel g, one can calculate an atomic density $\rho_{N_L}^g(t)$ for that sublevel by Eq. (15), where the pulse area θ_j is replaced by $\theta_j^g = -\int \Omega_g(t)dt$.

The total atomic density ρ^{tot} is the sum of contribution of each ground state,

$$\rho^{\mathrm{tot}} = \sum_g \rho^g. \tag{22}$$

The signal is obtained by scattering light from each ρ^g. We therefore must modify Eq. (16) to account for the different couplings of the ground states g to the light field. We obtain

$$\mathcal{E} \propto \mathcal{E}_0 \sum_{g,e} \rho_{-1}^g \frac{(\mathbf{d}_{eg}\cdot\boldsymbol{\sigma})(\mathbf{d}_{eg}\cdot\boldsymbol{\sigma}_s)}{2\Delta_{eg}}, \tag{23}$$

where $\boldsymbol{\sigma}_s$ is the polarization of the scattered field. The signal expressed by Eq. (23) still takes the form of Eq. (17), but $\mathcal{A}$ is replaced by

$$\mathcal{A}' = \sum_g w_g \prod_{j=2}^{L} J_{N_j - N_{j-1}}(2\theta_j^g \sin\varphi_j^{\mathrm{rec}}(t_{\mathbf{N}}^{\mathrm{echo}})), \tag{24}$$

where $w_g \equiv \Sigma_e (\mathbf{d}_{eg}\cdot\boldsymbol{\sigma})(\mathbf{d}_{eg}\cdot\boldsymbol{\sigma}_s)/(2\Delta_{eg})$. Equation (24) with appropriate atomic parameters for Rb was used to fit the data in Fig. 9.

VI. CONCLUSION

We have employed a de Broglie wave interferometry technique for generating and detecting density gratings in an atomic cloud. The period of these gratings is an even fraction of the optical wavelength λ. As a first step in exploring this method, we have observed structures of period $\lambda/2$ and $\lambda/4$ in a sample of $\sim$100-μK ^{85}Rb atoms. The $\lambda/2$ structures are observed *in situ* by scattering of a probe optical beam off them. The higher-order structures, such as the one with period $\lambda/4$, do not satisfy the phase-matching condition and thus do not scatter the probe field. To detect them, we developed a three-pulse echo technique, which renders a $\lambda/2N$ structure visible in real time by converting it to a $\lambda/2$ structure that can be interrogated by the scattering of a probe field. The data collected show good agreement with theory for a variety of experimental conditions and suggest a promising technique for on-line monitoring and control of atom lithography. We also look forward to extending our technique for creating and observing spatial gratings of smaller periods as well as to using it for atomic beam lithography.

ACKNOWLEDGMENTS

We thank Boris Dubetsky and Paul Berman for useful discussions. We acknowledge the financial support from the U. S. Army Research Office through Grant Nos. DAAD19-00-1-0412 and DAAD19-99-1-0033 and from the Packard Foundation.

[1] *Atom Interferometry*, edited by P.R. Berman (Academic Press, Cambridge, 1997).
[2] Quantum Semiclassic. Opt. **8**, 497 (1996), special issue on atom optics, edited by A. Arimondo and H.-A. Bachor.
[3] M. Kasevich and S. Chu, Phys. Rev. Lett. **67**, 181 (1991).
[4] M. Kasevich and S. Chu, Appl. Phys. B: Photophys. Laser Chem. **54**, 321 (1992).
[5] J.M. McGuirk, M.J. Snadden, and M.A. Kasevich, Phys. Rev. Lett. **85**, 4498 (2000).
[6] M.J. Snadden, J.M. McGuirk, P. Bouyer, K.G. Haritos, and M.A. Kasevich, Phys. Rev. Lett. **81**, 971 (1998).
[7] D.S. Weiss, B.C. Young, and S. Chu, Phys. Rev. Lett. **70**, 2706 (1993).
[8] D.S. Weiss, B.C. Young, and S. Chu, Appl. Phys. B: Lasers Opt. **59**, 217 (1994).
[9] J. Schmiedmayer, M.S. Chapman, C.R. Ekstrom, T.D. Hammond, S. Wehinger, and D.E. Pritchard, Phys. Rev. Lett. **74**, 1043 (1995).
[10] A. Lenef, T.D. Hammond, E.T. Smith, M.S. Chapman, R.A. Rubenstein, and D.E. Pritchard, Phys. Rev. Lett. **78**, 760 (1997).
[11] T.L. Gustavson, P. Bouyer, and M.A. Kasevich, Phys. Rev. Lett. **78**, 2046 (1997).
[12] G. Timp, R.E. Behringer, D.M. Tennant, J.E. Cunningham, M. Prentiss, and K.K. Berggren, Phys. Rev. Lett. **69**, 1636 (1992).
[13] J.J. McClelland, R.E. Scholten, E.C. Palm, and R.J. Celotta, Science **262**, 877 (1993).
[14] W.G. Kaenders, F. Lison, A. Richter, R. Wynands, and D. Meschede, Nature (London) **375**, 214 (1995).
[15] R.W. McGowan, D.M. Giltner, and S.A. Lee, Opt. Lett. **20**, 2535 (1995).
[16] R. Gupta, J.J. McClelland, P. Marte, and R.J. Celotta, Phys. Rev. Lett. **76**, 4689 (1996).
[17] T.W. Mossberg, R. Kachru, E. Whittaker, and S.R. Hartmann, Phys. Rev. Lett. **43**, 851 (1979).
[18] R. Beach, S.R. Hartmann, and R. Friedberg, Phys. Rev. A **25**, 2658 (1982).
[19] R. Friedberg and S.R. Hartmann, Phys. Rev. A **48**, 1446 (1993).
[20] B.Y. Dubetskii, A.P. Kazantsev, V.P. Chebotaev, and V.P. Yakovlev, Pis'ma Zh. Eksp. Teor. Fiz. **39**, 531 (1984) [JETP Lett. **39**, 649 (1984)].

[21] *Atom Interferometry*, (Ref. [1]).
[22] C.S. Adams, M. Sigel, and J. Mlynek, Phys. Rep. **240**, 143 (1994).
[23] T.W. Mossberg and S.R. Hartmann, Phys. Rev. A **23**, 1271 (1981).
[24] S.B. Cahn, A. Kumarakrishnan, U. Shim, T. Sleator, P.R. Berman, and B. Dubetsky, Phys. Rev. Lett. **79**, 784 (1997).
[25] L. Allen and J. Eberly, *Optical Resonance and Two-Level Atoms* (Wiley, New York, 1975).
[26] M.K. Oberthaler, S. Bernet, E.M. Rasel, J. Schmiedmayer, and A. Zeilinger, Phys. Rev. A **54**, 3165 (1996).
[27] B. Dubetsky and P.R. Berman, Phys. Rev. A **50**, 4057 (1994).
[28] M.S. Chapman, C.R. Ekstrom, T.D. Hammond, J. Schmiedmayer, B.E. Tannian, S. Wehinger, and D.E. Pritchard, Phys. Rev. A **51**, R14 (1995).
[29] S. Nowak, C. Kurtsiefer, C. David, and T. Pfau, Opt. Lett. **22**, 1430 (1997).
[30] C. Monroe, W. Swann, H. Robinson, and C. Wieman, Phys. Rev. Lett. **65**, 1571 (1990).
[31] J. Dalibard and C. Cohen-Tannoudji, J. Opt. Soc. Am. B **6**, 2023 (1989).
[32] D.S. Weiss, E. Riis, Y. Shevy, P.J. Ungar, and S. Chu, J. Opt. Soc. Am. B **6**, 2072 (1989).
[33] S.B. Cahn, Ph.D. thesis, State University of New York, Stony Brook, 1997.
[34] C. Cohen-Tannoudji, J. Dupon-Roc, and G. Grynberg, *Atom-Photon Interaction: Basic Processes and Applications* (Wiley, New York, 1992).
[35] When computing $|\psi_{\mathbf{v}_0}(\mathbf{x},t)|^2$ from Eq. (10), one encounters a series of the Bessel functions, on which the identity $\Sigma_{n=-\infty}^{+\infty} e^{i2An} J_n(\theta) J_{n+\delta}(\theta) = i^{\delta} e^{-i\delta A} J_{\delta}(2\theta \sin A)$ can be used.